Published in final edited form as:

Nat Struct Mol Biol. 2015 August ; 22(8): 603–610. doi:10.1038/nsmb.3053.

Recognition of Microbial Glycans by Human Intelectin

Darryl A. Wesener[1], **Kittikhun Wangkanont**[2], **Ryan McBride**[3,4], **Xuezheng Song**[5,6], **Matthew B. Kraft**[2,8], **Heather L. Hodges**[2], **Lucas C. Zarling**[1], **Rebecca A. Splain**[2,8], **David F. Smith**[5,6], **Richard D. Cummings**[5,6], **James C. Paulson**[3,4], **Katrina T. Forest**[7], and **Laura L. Kiessling**[1,2]

[1]Department of Biochemistry, University of Wisconsin–Madison, Madison, WI 53706, USA

[2]Department of Chemistry, University of Wisconsin–Madison, Madison, WI 53706, USA

[3]Department of Cell and Molecular Biology, The Scripps Research Institute, La Jolla, California 92037, USA

[4]Department of Chemical Physiology, The Scripps Research Institute, La Jolla, California 92037, USA

[5]Department of Biochemistry, Emory University School of Medicine, Atlanta, GA30322, USA

[6]Glycomics Center, Emory University School of Medicine, Atlanta, GA30322, USA

[7]Department of Bacteriology, University of Wisconsin–Madison, Madison, WI 53706, USA

Abstract

The glycans displayed on mammalian cells can differ markedly from those on microbes. Such differences could, in principle, be read by carbohydrate-binding proteins, or lectins. We used glycan microarrays to show that human intelectin-1 (hIntL-1) does not bind known human glycan epitopes but interacts with multiple glycan epitopes found exclusively on microbes: β-linked D-galactofuranose (β-Gal*f*), D-phospho-glycerol-modified glycans, heptoses, D-*glycero*-D-*talo*-oct-2-ulosonic acid (KO) and 3-deoxy-D-*manno*-oct–2-ulosonic acid (KDO). The 1.6 Å resolution crystal structure of hIntL-1 bound to β-Gal*f* revealed that hIntL-1 uses a bound calcium ion to coordinate terminal exocyclic 1,2-diols. N-Acetylneuraminic acid (Neu5Ac), a sialic acid widespread in human glycans, possesses an exocyclic 1,2-diol but does not bind hInt-1, likely due to unfavorable steric and electronic effects. Human IntL-1 marks only *Streptococcus pneumoniae*

Correspondence should be addressed to L.L.K. (kiessling@chem.wisc.edu).

[8]Present Addresses: Gilead Sciences, Inc., Foster City, CA 94404, USA (MBK). Global API Chemistry, GlaxoSmithKline, King of Prussia, PA 19406, USA (RAS).

Accession codes. Coordinates and structure factors have been deposited in the Protein Data Bank under accession codes 4WMQ (apo–hIntL-1) and 4WMY (Gal*f*-bound hIntL-1).

AUTHOR CONTRIBUTIONS

D.A.W and L.L.K. conceived the project. D.A.W., K.W., and L.L.K. planned the experiments, analyzed the data, and wrote the paper, with input from all the other authors. Cloning, protein expression, and biochemical experiments were performed by D.A.W. and L.C.Z. Microscopy was performed by H.L.H. Baculovirus was made by K.W. The carbohydrate ligands used were synthesized, and characterized by M.B.K., and R.A.S. The furanoside glycan microarray was constructed and analyzed with the mammalian glycan microarray by X.S., D.F.S., and R.D.C. The microbial glycan array was constructed and analyzed by R.M. and J.C.P. Protein crystallization and structure determination was performed by K.W. and K.T.F.

serotypes that display surface glycans with terminal 1,2-diol groups. This ligand selectivity suggests hIntL-1 functions in microbial surveillance.

Organisms that serve as hosts for microbes must distinguish microbial cells from those of their own[1,2]. A mechanism of differentiation is especially important at sites in which host tissues contact the environment, such as in the lung, intestine, and skin[3,4]. Differences in cellular surface glycosylation can serve as markers of a cell's identity—its developmental state, its tissue type, or whether it is self or non-self[5]. Cell surface glycans can be distinguished by carbohydrate binding proteins or lectins[6], which are typically categorized based on their monosaccharide selectivity[7]. These lectins can be exploited for host defense, as in the case of innate immune lectins, such as mannose-binding lectin (MBL)[8]. In the serum, MBL is precomplexed with mannose-binding lectin-associated serine proteases (MASPs), and interaction of this complex with a cell surface results in activation of the lectin pathway of complement, ultimately leading to pathogen opsonization and clearance[9,10]. Other humoral lectins implicated in immunity include ficolins, collectins, galectins, and HIP/PAP[1,11–13].

One group of lectins whose specificity remains unclear is that composed of intelectins (IntLs). The first IntL protein was reported in *Xenopus laevis* oocytes[14]. Homologs have since been identified in many other chordates; including other amphibians, fishes, and many mammals,. IntLs belong to a family of lectins termed X-type lectins[15] and have been shown to exist as homooligomers of 35 kDa monomers. They are reported to function as calcium ion-dependent lectins; however, they do not contain the calcium-dependent C-type lectin sequence motif[16] present in many human lectins. IntLs instead contain a fibrinogen like domain (FBD, residues 37–82 in hIntL-1 (ref. 17) and are proposed to be most similar to ficolins, a class of FBD-containing innate immune lectins[11].

Several observations implicate IntLs in innate immunity. Mammalian IntLs are predominantly produced by lung and intestinal goblet cells, and intestinal paneth cells[17–19]. In sheep and mice, IntL expression increases upon infection with intestinal parasitic nematodes[20,21]. In humans, the mucus induced by allergic reactions is enriched in IntLs[22,23]. Still, hIntL-1 has been reported to be the intestinal lactoferrin receptor[24], to function as a tumor marker.[25] It also be suggested to be involved in metabolic disorders including diabetes, where it is known as omentin[26]. Given these diverse potential functions, we set out to examine the ligand specificity of hIntL-1.

Human IntL-1 has been reported to bind furanose residues (5-membered ring saccharide isomers), including ribofuranose (Rib*f*) and a β-Gal*f*-containing disaccharide[17,27]. The monosaccharide Gal*f* is present in the cell surface glycans produced by a number of microbes, but the biosynthetic enzymes that mediate Gal*f* incorporation are absent in humans[28–30]. The presence of Gal*f* in microbial glycans but not in those of humans is an example of phylogenetic glycan differences[31]. This is just one example, as collectively the surface glycans of microbes are generated from more than 700 unique building blocks, while less than 35 carbohydrate residues are needed to assemble mammalian glycans[32,33]. In principle, targeting monosaccharide residues unique to microbes could be used by the innate immune system to differentiate mammalian cells from microbes.

We reasoned that clues to hIntL-1 function would emerge from determining the glycans it binds and the molecular basis for its recognition selectivity. Here, we use glycan microarrays to demonstrate that hIntL-1 binds microbial over human glycans. Given the diversity of microbial glycans, a lectin that binds a single microbial saccharide epitope (e.g., galactofuranose) would be expected to have specialized function. It is therefore striking that hIntL-1 does not engage a single monosaccharide or even related saccharides; rather, hIntL-1 interacts with multiple, structurally divergent microbial monosaccharide residues. The molecular mechanism by which hIntL-1 recognizes its targets was revealed by X-ray crystallography: hIntL-1 binds its carbohydrate ligands through calcium ion-dependent coordination of a conserved exocyclic, terminal 1,2-diol. The functional group selectivity observed in the glycan arrays is manifested in the context of cells, as hIntL-1 targets *S. pneumoniae* serotypes that display its glycan ligands.

RESULTS

hIntL-1 binds β-Gal*f*

Native hIntL-1 has been shown to exist as a disulfide-linked trimer[17,27]. Therefore, we first developed a robust expression system that yields the protein as a disulfide-linked trimer that could be purified using an immobilized β-Gal*f* column (Supplementary Fig. 1a and b). Because lectin–carbohydrate interactions often depend on multivalent binding[34,35] we postulated that hIntL-1 trimers might bind avidly to multivalent carbohydrate displays. Human IntL-1 carbohydrate-binding specificity hence was evaluated using immobilized biotinylated carbohydrates (β-D-Gal*f*, β-D-galactopyranose (β-Gal*p*), β-D-ribofuranose (β-Rib*f*)) in an enzyme-linked immunoabsorbent-like assay (ELISA) (Fig. 1a and Supplementary Fig. 1c and d). The monosaccharide binding epitopes we tested were chosen based upon a previous study in which a small carbohydrate panel was evaluated for inhibition of hIntL-1 binding to an immobilized carbohydrate[17]. In those studies, ribose was the most effective competitor (IC_{50} < 5 mM) followed by Gal*f*-β(1,4)-GlcNAc (IC_{50} = 9 mM) with galactose being less potent (IC_{50} = 66 mM)[17]. Our data indicate that hIntL-1 does not bind ribofuranose nor galactopyranose, but it does engage the β-Gal*f*-substituted surface avidly with a functional affinity (apparent affinity) of 85 ±14 nM (Fig. 1b).

Our results contrast with those of the previous study[17], as we did not detect binding to the pyranose form of galactose nor to ribofuranose. The apparent discrepancies could arise because the previous investigation required high concentrations free carbohydrate. Under those conditions, competition could arise from protein modification or from the less prevalent open chain form of the saccharide. The apparent binding constant we observed for hIntL-1 binding to immobilized β-D-Gal*f* suggests that the protein binds tightly to a ligand, but the previous IC_{50} for the β-D-Gal*f*-containing disaccharide (9 mM) suggests the interaction is weak. This difference presumably stems from the distinct assay formats. We postulated that the presentation of glycosides from a surface is a more relevant assessment of hIntL-1 activity as it mimics key aspects of the multivalent display of carbohydrate ligands on a cell surface[34]. Still, the differences between the reported hIntL-1 binding specificities and those we observed prompted us to examine hIntL-1 binding using another assay. We used surface plasmon resonance (SPR) and monitored hIntL-1 interaction with

surfaces to which the aforementioned saccharides or β-D-arabinofuranose (β-Ara*f*) or α-L-rhamnopyranose (α-L-Rha) were appended. Even at high concentrations of hIntL-1, we observed only selective hIntL-1 binding to β-Gal*f* (Fig. 1c and Supplementary Fig. 1e).

hIntL-1 binding to microbial glycans

Glycan microarray technology afforded a more comprehensive assessment of hIntL-1 ligand recognition[36]. We prepared a focused array that included furanosides (Supplementary Table 1) using the methods employed in generating the Consortium for Functional Glycomics (CFG; http://www.functionalglycomics.org) mammalian glycan v5.1 array, and both arrays were tested for hIntL-1 binding. In the focused array, lacto-N-neotetraose (LNnT) and asialo, galactosylated bi-antennary N-linked glycan (NA2) were included to ascertain the efficiency of carbohydrate immobilization. Data from the focused array were consistent with those obtained from the ELISA and SPR assays, indicating that of the carbohydrates displayed, hIntL-1 bound only to those with β-Gal*f* residues (Fig. 2a and Supplementary Table 1). We attribute the small amount of binding to β-Gal*p* to its hydrophobic, alkyl anomeric linker. In contrast to the furanoside array, testing of the CFG v5.1 array yielded no validated interactions with mammalian glycans (Fig. 2a). Increasing the protein concentration yielded similarly low signals suggesting the modest residual binding detected arose from nonspecific interactions (Supplementary Table 2). Thus, none of the human glycans examined are ligands of hIntL-1.

The initial binding data revealing hIntL-1 robustly complexes β-Gal*f* residues but not human glycans prompted us to evaluate the lectin's specificity for a more diverse collection of microbial glycans. Though absent from mammals[28], Gal*f* residues occur in glycans from a number of human pathogens, including the bacteria *Mycobacterium tuberculosis* and *Klebsiella pneumoniae*, and the fungal pathogen *Aspergillus fumigatis*[29,37]. The possibility that hIntL-1 interacts with microbial glycans was tested using a microarray displaying more than 300 oligosaccharides from bacterial species[38]. Screening of this array revealed multiple glycan ligands for hIntL-1 (Fig. 2b and Supplementary Fig. 2a, Supplementary Table 3). These ligands encompassed glycans from Gram-negative and Gram-positive bacteria; including *S. pneumoniae*, *Proteus mirabilis*, *Proteus vulgaris*, *Yersinia pestis*, and *K. pneumoniae* (Table 1). Four of the top-fifteen ligands contained terminal β-Gal*f* epitopes, including outer polysaccharide (OPS) from *K. pneumoniae* and a capsular polysaccharide from *S. pneumoniae*. Surprisingly, the majority of the glycans identified did not possess Gal*f* residues. The top five hits had saccharide residues with D-glycerol-1-phosphate substituents. This epitope was the common feature, as the residue to which it was appended varied between glycans. Other common epitopes included either D/L-*manno*-heptose, KO, or KDO residues (Fig. 2c). Each characterized glycan ligand from the top 15 hits contains at least one of the five aforementioned epitopes. Despite its ability to bind structurally diverse glycans, hIntL-1 exhibited selectivity. Conspicuously missing from hit microbial glycan ligands were those containing α-Gal*f* residues (Supplementary Fig. 2b). What was especially notable, however, was that none of the hIntL-1 ligands we identified on the microbial glycan array are found in mammalian glycans, but collectively these five residues are widely distributed in bacteria[32].

Structure of hIntL-1

To understand the molecular mechanisms underlying glycan recognition by hIntL-1, we determined its structure using X-ray crystallography. Apo-hIntL-1 crystals diffracted to 1.8 Å resolution, and the structure of the protein was solved by molecular replacement using the structure of a selenomethione-labeled *Xenopus laevis* IntL as a search model (Table 2) (PDB ID: 4WMO). Human IntL-1 possesses an oblong, globular structure containing two highly twisted β sheet-containing structures surrounded by seven short α helixes and extensive random coil regions (Fig. 3a). The second of these β sheets structures closes on itself to form a very short stretch of unusually flattened β-ribbons (amino acids 221–226 + 248–278). A Dali search[39] using the hIntL-1 structure yielded several weak fibrinogen and ficolin structure hits (RMSD values ∼4 Å). The secondary structures of L-ficolin[40] and hIntL-1 are related up to residue 150, although the sequence conservation is limited to the FBD. The remaining residues diverge substantially in sequence and structure (Supplementary Fig. 3). Indeed, removal of the first 150 residues from the hIntL-1 Dali input yielded no hits. These data indicate hIntL-1 has a composite fold not previously reported.

Two hIntL-1 monomers are present in the asymmetric unit (Chain A and Chain B), and they represent two similar, though non-identical (Cα RMSD=0.65 Å), disulfide-linked trimers, each arranged around a crystallographic threefold axis. In one trimer, the peptide chain that connects each monomer to the adjacent monomer is resolved, such that the intermolecular disulfide bond between residues C31 and C48 is apparent (Fig. 3a). These data are consistent with SDS-PAGE analysis indicating the hIntL-1 exists as a trimer. Each hIntL-1 monomer has three calcium ions, and each cation is chelated exclusively by hard protein or water ligands (bond distance 2.3–2.5 Å). Two of these cations are embedded within the protein while one is surface exposed.

To determine how hIntL-1 binds its ligands, we solved a structure of the complex of allyl-β-D-Gal*f* bound to hIntL-1 to 1.6 Å resolution. The Cα RMSD between the asymmetric unit of apo- and Gal*f*–bound structures (0.118 Å) suggested no significant structural changes occur upon ligand binding. The Gal*f* O(5) and O(6) hydroxyl groups displace ordered water molecules and serve as coordinating ligands for the surface accessible calcium ion, with protein side chains poised for hydrogen bonding, (i.e., H263 to the Gal*f* o(6) hydroxyl group, Fig. 3b & Supplementary Fig. 4a) thereby enhancing calcium coordination. The carbohydrate vicinal exocyclic hydroxyl groups adopt a gauche conformation as they chelate the calcium, with dihedral angles of 45° and 51° for Chain A and B, respectively. As anticipated from the structure, glycans containing Gal*f* residues with substituents at either the O(5) or O(6) fail to bind hIntL-1 (Fig. 2b and Supplementary Table 3). This portion of the saccharide also fits well into a binding pocket formed by W288 and Y297. The presence of these aromatic groups suggests that CH–π bonds contribute to affinity.

The high resolution of the structure of the hIntL-1 complex allows unambiguous assignment of the β-Gal*f* ring conformation in each monomer (Supplementary Fig. 4b)[41,42]. Using the Altona-Sundaralingam pseudorotational model, we calculated the pseudorotational phase angle, P, of each furanoside to assign its conformation[43]. In hIntL-1 Molecule A, the furanoside is in the $^{1}T_{O}$-gg-gt (calculated P=105°) conformer, while the β-Gal*f* shown in

Fig. 3b adopts the ^{4}E-gg-gt (calculated P=57°) conformation (Supplementary Fig. 4c and 4d). The presence of conformational differences within the structures are consistent with the flexibility of furanosides[42].

Structural basis for hIntL-1 selectivity

The structure of the lectin-Gal*f* complex reveals why the acyclic 1,2-diol moiety is critical – the vicinal hydroxyl groups engage in calcium ion coordination. Still, other glycan properties contribute to hIntL-1 recognition. For example, hIntL-1 does not bind α-Gal*f* substituted glycans (Supplementary Fig. 2b). A cursory assessment of the β-Gal*f* complex suggests hIntL-1 might accommodate α-Gal*f* linkages. An alteration in anomeric configuration for furanosides, however, can drastically change conformational preferences. Although the low energetic barrier of furanoside ring pseudorotation complicates definitive analysis, experimental and computational studies of the isomeric methyl glycosides of D-Gal*f* have revealed that the anomers have dramatically different conformational preferences[42]. The β-Gal*f* ^{4}E-gg-gt conformer that we find in hIntL-1 Chain B is predicted to be the second lowest in energy (0.4 kcal/mol)[42]. That conformation for methyl-α-Gal*f* is destabilized by 3.2 kcal/mol. As a result, the expected Boltzmann population for methyl-α-Gal*f* in a ^{4}E-gg-gt conformation is less than 0.2%, ranking it 25th out of the 90 conformations examined[42]. These data suggest that α-Gal*f* residues adopt a conformation incompatible with favorable hIntL-1 interactions.

One of the most striking findings from the binding data is that the lectin failed to interact with any of the 148 α-Neu5Ac-containing glycans in the mammalian glycan array (Fig. 2a). A saccharide epitope widespread in human glycans, α-Neu5Ac residues have a terminal 1,2-diol and share similarity with 2-keto-3-deoxyoctonic acids (KDO), which are common in microbial glycans and do function as hIntL-1 ligands[44]. We used a biotinylated glycoside to confirm that hIntL-1 fails to interact with surfaces displaying α-Neu5Ac (Supplementary Fig. 5a). Moreover, compounds identified as hIntL-1 ligands—glycerol and glycerol-1-phosphate— competitively inhibit the lectin from binding to β-Gal*f*, but methyl-α-mannopyranoside and methyl-α-Neu5Ac do not (Supplementary Fig. 5b). These results indicate that hIntL-1 uses a single site to bind disparate sterically unhindered 1,2-diol epitopes within microbial glycans, yet the lectin evades interaction with human carbohydrate epitopes.

To understand the ability of hIntL-1 to discriminate between methyl-α-Neu5Ac and bacterial carboxylic acid-containing sugars such as KDO and KO, we docked methyl-α-Neu5Ac and methyl-α-KDO into the hIntL-1 structure. The KDO glycoside is readily accommodated, but the α-Neu5Ac glycoside is not (Fig. 4a and b). Anion – anion repulsion between the α-Neu5Ac anomeric exocyclic carboxylate and the carboxylate side chains in the binding site should destabilize binding. Additionally, steric interactions between the methyl group of the anomeric oxygen, and the bulky C(5) N-acetyl group with the protein surface should disfavor α-Neu5Ac complexation (Fig. 4a). The destabilizing interactions with α-Neu5Ac cannot be mitigated by rotating bonds or by adopting accessible low energy conformations. Future experiments using protein variants and ligand analogs will be useful in testing this proposed evasion mechanism.

hIntL-1 comparison with ficolins

The FBD of hIntL-1 suggested it would be related to the ficolins. With the structure of an X-type lectin complex, it is now apparent that, outside the FBD, intelectins and the ficolins deviate extensively. IntLs lack the collagen-like domain that mediates complement activation. Additionally, the hIntL-1 carbohydrate-recognition domain is larger than that of the ficolins, and hIntL-1 coordinates three calcium ions, two of which are buried, while the ficolins bind only a single calcium ion. Finally, the carbohydrate binding site and mode of recognition differ. The ficolin calcium ion is not found in the glycan-binding site; in contrast, a surface-exposed calcium ion in hIntL-1 participates directly in glycan binding (Supplementary Fig. 3c). Together, the data suggest that X-type lectins, of which the hIntL-1 structure serves as the founding member, constitute a distinct protein structural class.

hIntL-1 binding to *S. pneumoniae*

Based on the expression of hIntL-1 in mucosal tissues, we examined binding to immunologically distinct serotypes of the encapsulated human lung pathogen *S. pneumoniae*, the causative agent of several diseases, including pneumonia, meningitis, and septicemia[45]. The surface exposed pneumococcal capsular polysaccharide (CPS) is among the first microbial antigens encountered by the immune system upon challenge[46]. This capsule is important for pathogen survival and is associated with virulence. Antibodies targeting the capsule have been shown to be protective against pneumococcal diseases, an observation that was leveraged to develop a polysaccharide-based vaccine that is protective against streptococcus infections[47]. The serotypes that we selected possess glycans that were present on the microbial glycan array: serotype 8 displays a glycan that lacks a terminal diol, serotype 43 displays a phosphoglycerol unit, and serotypes 20 and 70 possess β-Gal*f* residues (Fig. 5a)[46]. The data indicate that hIntL-1 binds to the surface of serotypes 20, 70 and 43, each of which displays cell surface glycans with an exocyclic, terminal 1,2-diol (Fig. 5b–d and Supplementary Fig. 6). As predicted by the β-Gal*f*–hIntL-1 complex structure, binding to these strains depends on calcium ion-mediated coordination, and glycerol functions as a competitive ligand (Fig. 5b and d). The relative fluorescence intensity of hIntL-1 binding to whole bacteria is generally consistent with the results predicted by the microbial glycan array. Specifically, hIntL-1 bound to strains that display β-Gal*f* (i.e., hit 13 from the microbial array, Table 1), but it interacted most avidly with the serotype displaying the D-glycerol-1-phosphate-modified saccharide that was the top hit from the microbial glycan array (Fig. 5c). These data suggest that the relative ligand ranking from the array analysis can provide information about how effectively a lectin can target cells displaying those glycans. Moreover, the results demonstrate that hIntL-1 specifically recognizes structurally diverse exocyclic 1,2-diol containing glycans on the surface of bacteria.

Human IntL-1 has been reported to bind lactoferrin,[24] a protein that appears to have antimicrobial activity[48]. These observations suggest that hIntL-1 could recruit lactoferrin to microbial cell surfaces for cell killing. To examine the interaction between these proteins, we immobilized human lactoferrin and assayed hIntL-1 binding by ELISA. As reported, we detected an interaction between lactoferrin and hIntL-1, but in contrast to the previous reports, in our assay, this interaction did not require calcium ions. The apparent affinity we measured for the hIntL-1 trimer is rather weak for a specific protein–protein interaction

(K_d∼500 nM). The isoelectric points (pI) of the proteins, pI∼5.5 for hIntL-1 and pI∼8.5 for lactoferrin, suggest the interaction may be mediated by bulk Coulombic interactions. We were unable to detect any killing of *S. pneumoniae* by human lactoferrin (up to 100 μg/mL) in a buffer that would be compatible with hIntL-1 binding the cell surface (HEPES buffered saline, pH 7.4, with 2 mM $CaCl_2$). Our results were consistent with those of others who noted that under similar conditions, the bactericidal activity of lactoferrin is abolished[49,50]. These initial results are inconsistent with a central role for lactoferrin–intelectin complexes mediating microbial cell killing, and they suggest other functional roles for hIntL-1 should be explored.

Murine IntL-1 binding to Gal*f*

If the role of intelectins is to participate in defense against microbes, the recognition specificity of intelectins from other mammals should be preserved. We therefore produced murine IntL-1, which is the mouse homolog[27] of hIntL-1. When murine IntL-1 was tested using the SPR assay used with the human homolog, its glycan recognition properties were analogous: It failed to interact with β-ribofuranose, β-arabinofuranose, α-rhamnopyranose, or β-Gal*p*, but it did interact with β-Gal*f* (Supplementary Fig. 7a). These data support the prospect that IntLs from different species have evolved to bind widely distributed 1,2-diol-containing epitopes unique to microbes.

DISCUSSION

Data from glycan microarrays reveal that hIntL-1 recognizes multiple microbial glycan epitopes yet paradoxically can discriminate between microbial and mammalian glycans. By determining the structure of this X-type lectin bound to Gal*f*, this apparent contradiction was resolved. The five common saccharide epitopes identified as recognition motifs (Gal*f*, phosphoglycerol, glycero-D-manno-heptose, KDO, and KO) share a common feature: a terminal acyclic 1,2-diol group. The hIntL-1 X-ray structure indicates that these terminal vicinal hydroxyl groups can coordinate to a protein-bound calcium ion. This binding mode has similarities to that employed by another major class of mammalian carbohydrate-binding proteins: the C-type lectins[16]. C-Type lectins also recognize glycans through calcium ions in the binding site to which carbohydrate hydroxyl groups coordinate[7]. In the case of C-type lectins, however, the hydroxyl groups employed are typically those on the pyranose ring of a mannose or fucose residue. The hIntL-1 binding pocket requires that any 1,2-diol motifs possess a primary hydroxyl group, as the aromatic substituents W288 and Y297 act as walls to preclude the binding of more substituted diols. These aromatic substituents presumably not only contribute to specificity but also to affinity. Their positioning should allow them to participate in CH–π interactions[51] which would enhance binding.

Although the terminal 1,2-diol is necessary for hIntL-1 recognition, it is not sufficient. The lectin is unable to bind human glycans, including those with an α-Neu5Ac residue. This result was confusing as glycans with α-Neu5Ac residues were prevalent on the mammalian glycan microarray, and although many glycans in this array present a terminal 1,2 diol, none were bound by hIntL-1 We were unable to model methyl-α-Neu5Ac in the hIntL-1 binding site without incurring Coulombic repulsion or severe steric interactions. These observations

suggest a molecular basis for hIntL-1's ability to avoid interaction with human glycans. With a structure that identifies the glycan-binding site, the proposed rationale for hIntL-1's selectivity for microbial glycans can be tested further.

We anticipate our structure will also provide insight into the physiological roles of the intelectins. The upregulation of intelectins upon infection suggests they may function in innate immunity. Although existing data from genome-wide association studies do not directly link intelectin mutations and increased susceptibility to infection, there are studies linking hIntL-1 to asthma[52] and Crohn's disease[53]. These diseases arise from defects at mucosal surfaces where intelectins are secreted. In relation to asthma, the amino acid variant V109D was identified with an increased risk[52]. Our structure reveals that this residue is not centrally important for binding, but it is located at a monomer–monomer interface.

We postulate that the trimeric form of hIntL-1 is important for the lectin's function. The presence of three binding sites on one face of the hIntL-1 trimer (Fig. 3a) suggested the protein could exploit multivalency to recognize relevant terminal 1,2 diol motifs and bind avidly to microbes. We therefore tested whether hIntL-1's selectivity for glycans would be manifested in a proclivity to engage only those *S. pneumoniae* serotypes whose capsular polysaccharides possess hIntL-1 recognition motifs. Our finding that hIntL-1 bound to strains bearing Gal*f* (serotypes 20 or 70) or phosphoglycerol (serotype 43) but not those lacking the requisite terminal 1,2-diol (serotype 8) highlights the advantages of using a simple binding epitope: Human IntL is not restricted to binding solely one glycan building block, rather it can interact with bacterial cells that present glycans composed of very different components (Gal*f* versus phosphoglycerol).

Because it engages a small epitope found within microbial glycans, hIntL-1 should be capable of recognizing a wide variety of microbes. Analysis of the twenty most common glycan building blocks unique to microbes indicates that half of these possess an acyclic1,2-diol that could, in principle, be recognized by intelectins (Fig. 6)[32]. The potential that a given microbe generates glycan ligands for hIntL-1 can be inferred from genetic sequence data. For example, organisms bearing Gal*f* residues harbor a *glf* gene[29]. D-Glycerol-1-phosphate-modified glycans are generated using CDP-D-glycerol as an activated donor and therefore will encode functional homologs of the *S. pneumoniae gct* gene[46]. Pathways that lead to the incorporation of heptose, KO, and KDO are known, as these residues are found in lipopolysaccharide (LPS)[54] and capsular (K-) antigen of Gram-negative bacteria[55]. The orientation of the saccharide binding sites on a single face of the hIntL-1 trimer not only can enhance the avidity of cell-surface binding, it also provides a surface for recruitment of other immune proteins or effectors to a hIntL-1-bound microbe. The remarkable selectivity of hIntL-1 for microbial over human cell surface glycans raises the intriguing possibility that IntLs function as microbial detectors. It is possible that this selective microbial recognition can be harnessed to deliver cargo to microbes, to detect them, or to target them for destruction.

ONLINE METHODS

Chemical synthesis of glycans

Procedures for glycan synthesis are included and described in detail in the Supplementary Note.

Native human intelectin-1 expression and purification

The cDNA for hIntL-1 (Accession Number: NM_017625) was obtained from Open Biosystems Clone LIFESEQ2924416 as a glycerol stock (GE Healthcare). The full coding sequence, residues 1–313, was amplified using PCR with the forward primer 5'-CGTGGGATCCTGGAGGGAGGGAGTGAAGGAGC-3' and the reverse primer 5'-GCCAGCTCGAGACCTTGGGATCTCATGGTTGGGAGG-3'. The primers installed sites for the restriction endonucleases *BamHI* and *XhoI*, respectively. The doubly digested PCR fragment encoding hIntL-1 was ligated into a doubly digested pcDNA4/*myc*-HisA vector backbone (Life Technologies). Correct insertion was confirmed with DNA sequencing (UW-Madison Biotechnology Center).

The hIntL-1 gene was expressed via transient transfection of suspension adapted HEK 293T cells obtained from the American Tissue Culture Collection (ATCC). Cells were transfected in Opti-mem I Reduced Serum Medium (Life Technologies) at ~2_E6 cells/mL using Lipofectamine 2000 (Life Technologies), according to the manufacturers protocol. Six hours post transfection, the culture medium was exchanged to FreeStyle F17 expression medium (Life Technologies) supplemented with 50 U/mL penicillin-streptomycin, 4 mM $_L$-glutamine, 1x nonessential amino acids, 0.1% fetal bovine serum (FBS) and 0.1% Pluronic F-68 (Life Technologies). Cells expressing hIntL-1 were cultured for up to 6 days, or until viability decreased below 60%, at which point the conditioned expression medium was harvested by centrifugation and sterile filtration.

Conditioned medium was adjusted to pH 7.4 by slow addition of a 0.1 M solution of sodium hydroxide (NaOH), and calcium chloride ($CaCl_2$) was added from a 1 M stock solution to achieve a final concentration of 10 mM. Recombinant hIntL-1 was purified by binding to a β-Gal*f* column generated from reaction of a β-Gal*f* glycoside bearing an anomeric linker and an amine to UltraLink Biosupport (Piere). The resulting resin was washed with a solution of 20 mM HEPES (7.4), 150 mM sodium chloride (NaCl), and 10 mM $CaCl_2$. Human IntL-1 was eluted with a solution of 20 mM HEPES (7.4), 150 mM NaCl, and 10 mM ethylenediaminetetraacetic acid (EDTA), and the protein was concentrated using a 10,000 molecular weight cut-off (MWCO) Amicon Ultra Centrifugal Filter. The buffer was exchanged to 20 mM HEPES (7.4), 150 mM NaCl, and 1 mM EDTA. Protein purity was assessed by SDS-PAGE electrophoresis and Coomassie blue staining, and was often >95%. The concentration of hIntL-1 was determined using absorbance at 280 nm with a calculated ε=237,400 $cm^{-1}M^{-1}$ for the trimer, and an estimated trimer molecular mass of 101,400 Da (to account for glycosylation). Typical yields from a 30 mL transfection were 400 μg.

Expression and purification of *strep*-tag® II hIntL-1

An N-terminal *Strep*-tag® II was cloned into the hItnL-1::pcDNA4 vector using site-directed mutagenesis and a primer set comprised of 5'-ACCACCAGAGGATGGAGTACAGATTGGAGCCATCCGCAGTTTGAAAAGTCTACAGATGAGGCTAATACTTACTTCAAGGA-3' and its reverse complement. The correct insertion was confirmed with DNA sequencing. *Strep*-hIntL-1 was expressed identically to hIntL-1. For purification, conditioned *Strep*-hIntL-1 medium was adjusted to pH=7.4 using NaOH, avidin was added per the IBA GmbH protocol (IBA GmbH, cat. no. 2–0205–050), $CaCl_2$ was added to 10 mM, and the solution was cleared with centrifugation (15,000*g* for 15 minutes). Protein was captured onto 2 mL of *Strep*-Tactin Superflow resin (IBA GmbH, cat. no. 2–1206–002). The resulting resin was washed with a solution of 20 mM HEPES (7.4), 150 mM NaCl, and 10 mM $CaCl_2$ and then 20 mM HEPES (7.4), 150 mM NaCl, and 1 mM EDTA. The protein was eluted with 5 mM d-desthiobiotin (Sigma) in 20 mM HEPES (7.4), 150 mM NaCl, and 1 mM EDTA and concentrated using a 10,000 MWCO Amicon Ultra Centrifugal Filter. The concentration of *Strep*-hIntL-1 was determined using absorbance at 280 nm with a calculated ε=237,400 $cm^{-1}M^{-1}$ for the trimer, and an estimated trimer molecular mass of 101,400 Da. Typical yields were similar to what was measured with untagged hIntL-1.

For protein X-ray crystallography, *Strep*-hIntL-1 was purified following culture medium dialysis against 20 mM BIS-TRIS (6.7), 150 mM NaCl, and 1 mM EDTA. The pH of the culture medium was adjusted to 6.7, avidin was added per the IBA GmbH protocol, $CaCl_2$ was added to 10 mM and the solution was cleared with centrifugation. Protein was purified by capture onto *Strep*-Tactin Superflow resin. Resin was washed with 20 mM BIS-TRIS (6.7), 150 mM NaCl, 10 mM $CaCl_2$ and then 20 mM BIS-TRIS (6.7), 150 mM NaCl, 0.5 mM EDTA. Protein was eluted with 5 mM d-desthiobiotin (Sigma) in 20 mM BIS-TRIS (6.7), 150 mM NaCl, 0.5 mM EDTA and concentrated using a 10,000 MWCO Amicon Ultra Centrifugal Filter.

hIntL-1 carbohydrate binding ELISA-like assay

To fabricate carbohydrate-displaying surfaces, 0.5 μg of streptavidin (Prozyme, cat. no. SA20) was adsorbed onto a Maxisorp (Nunc) flat bottom 96 well plate in phosphate-buffered saline (PBS). Wells were washed with PBS and then coated with 5 μM of carbohydrate–biotin ligand in PBS for 1 hour at 22 °C. Wells were blocked with bovine serum albumin (BSA) in ELISA buffer (20 mM HEPES (7.4), 150 mM NaCl, 10 mM $CaCl_2$, and 0.1% Tween-20). Samples containing hIntL-1 were prepared by serial dilution into ELISA buffer + 0.1% bovine serum albumin (BSA) and added to wells for 2 hours at 22 °C. Wells were washed four times with ELISA buffer. Bound hIntL-1 was detected using 0.75 μg/mL of a sheep polyclonal IgG hIntL-1 antibody (R&D Systems, cat. no. AF4254) in ELISA buffer + 0.1% BSA for 2 hours at 22 °C. This primary antibody has been validated by the company for detecting intelectin by Western blot, immunohistochemistry, and direct ELISA. Wells were washed with ELISA buffer. A donkey anti-sheep IgG horseradish peroxidase (HRP) conjugate (Jackson ImmunoResearch Laboratories) was added at a 1:5,000 dilution in ELISA buffer + 0.1% BSA for 1 hour at 22 °C. When *Strep*-hIntL-1 was assayed, StrepMAB-Classic HRP conjugate (IBA GmbH, cat. no. 2–1509-001) was used to

specifically recognize the Strep-tag® II of bound hIntL-1. StrepMAB-Classic HRP conjugate was diluted 1:10,000 in ELISA buffer + 0.1% BSA and incubated for 2 hours at 22 °C. Wells were washed. Human IntL-1 was detected colorimetrically with addition of 1-Step Ultra TMB-ELISA (Pierce). Once sufficient signal was achieved (typically < 2 minutes), the reaction was quenched with addition of equal volume of 2 M sulphuric acid (H_2SO_4). Plates were read at 450 nm on an ELx800 plate reader (Bio-Tek). When testing the calcium ion dependency of hIntL-1, 1 mM EDTA replaced 10 mM $CaCl_2$ in all steps. Data were analyzed on Prism6 (GraphPad). Data were fit to the one site binding equation.

Surface plasmon resonance (SPR)

Analysis of intelectins using SPR was conducted on a ProteOn XPR36 (Bio-Rad) at the University of Wisconsin–Madison Department of Biochemistry Biophysics Instrumentation Facility (BIF). To measure intelectin binding, ProteOn NLC sensor chips (NeutrAvidin coated sensor chip) (Bio-Rad, cat. no. 176–5021) were used to capture the biotinylated carbohydrate ligand. All experiments presented here were conducted at surface saturated levels of ligand, ∼200 response units (RU). In all experiments, captured biotin was used in flow cell one as a control. Samples containing purified intelectin were prepared by serial dilution into intelectin SPR running buffer (20 mM HEPES (7.4), 150 mM NaCl, 1 mM $CaCl_2$, and 0.005 % Tween-20). Surfaces were regenerated with short injections of solutions of 10 mM hydrochloric acid (HCl). Data were referenced using either the interspots or the biotin reference channel, and processed using the Bio-Rad ProteOn software package.

Construction of the furanoside glycan array

The microarray of furanoside containing glycans was printed as previously described[61,62]. Briefly, the amine functionalized glycans shown in Fig. s6A were dissolved in 100 mM sodium phosphate (8.0) and printed as 14 arrays on N-hydroxysuccinimidyl (NHS) ester-activated slides (Shott Nexterion, Louisville, KY). Arrays were printed in replicates of n=4 at different glycan concentrations (as indicated in Fig. s6B) using a Piezorray printer (Perkin Elmer, Waltham, MA) that delivered 0.33 nL per spot. The 2-amino(N-aminoethyl) benzamine (AEAB) derivatives of lacto-N-neotetraose (LNnT) and asialo, galactosylated bi-antennary N-linked glycan (NA2) were printed as controls to confirm glycan immobilization. After printing, covalent coupling of glycans to the surface was facilitated by incubation at 55 °C in an atmosphere of >80% humidity for 1 hour. Slides were dried in a desiccator overnight and blocked using a solution of 50 mM ethanolamine in 50 mM borate buffer (8.0). Prior to interrogating with glycan binding proteins (GBPs), the arrays are rehydrated in binding buffer.

Assay of hIntL-1 on furanoside and CFG mammalian glycan array

GBPs at various concentrations were applied to separate furanoside arrays in 70 μL of binding buffer (20 mM HEPES (7.4), 150 mM NaCl, 1 mM EDTA, 10 mM $CaCl_2$, 1% BSA and 0.05% Tween-20) in the wells formed on the slide with a silicon grid (14 wells per slide). After incubation for 1 hr at RT, the slides were washed with wash buffer (20 mM HEPES (7.4), 150 mM NaCl, 1 mM EDTA and 10 mM $CaCl_2$, 0.05% Tween-20). The biotinylated lectins *Erythrina cristagalli* lectin (ECL) and *Ricinus communis* agglutinin I

lectin (RCA-I) were detected using Alexa Fluor® 488-labeled streptavidin (10 μg/ml) in binding buffer (Fig. s6C and D). hIntL-1 was detected with a sheep polyclonal IgG antibody specific for hIntL-1 (5 μg/ml) (R&D Systems) and an Alexa Fluor® 488-labeled donkey anti-sheep IgG secondary antibody (5 μg/ml) (Life Technologies). Bound protein was detected using a ProScanArray Scanner (Perkin Elmer) equipped with 4 lasers covering an excitation range from 488 to 633 nm. The data from the furanoside glycan array were analyzed with the ScanArray Express software (Perkin Elmer) as the average of the 4 replicates.

For the analysis of the CFG glycan array[36], hIntL-1 was applied in 70 μl at a concentration of 50 and 200 μg/ml in binding buffer under a coverslip to distribute the solution evenly over the large array of 610 glycans printed in replicates of n=6 (Array v5.1). After washing and scanning, the data from the CFG glycan microarray were analyzed using ImaGene software (BioDiscovery, Hawthorne, CA) as the average of 4 values after removing the high and low values of the 6 replicates. With both the furanoside and mammalian glycan array, the images were converted to Excel files, and the data are reported as histograms of average Relative Fluorescence Units (RFU) versus print identification number that identified the glycan targets. Figures were made using Prism6 (GraphPad) or Excel (Microsoft).

Assay of hIntL-1 on the bacterial glycan array

Strep-hIntL-1 was used to interrogate the Microbial Glycan Microarray version 2 (MGMv2). Construction of the MGMv2 is previously described[38]. Briefly, bacterial polysaccharide samples were dissolved and diluted to 0.5 mg/mL in printing buffer (150 mM sodium phosphate buffer (8.4) + 0.005% Tween-20). Samples were immobilized on NHS-activated glass slides (SlideH, Schott/Nexterion) using a MicroGrid II (Digilab) contact microarray printer equipped with SMP-4B printing pins (Telechem). Six replicates of each bacterial glycan sample were printed. Covalent coupling of glycans to the surface was facilitated by incubation for 1 hour post-print at 100% relative humidity. The remaining reactive NHS-moieties were quenched using a blocking solution (50 mM ethanolamine in 50 mM borate buffer (9.2)). Blocked slides were stored at −20 °C until assays were performed.

To interrogate the MGMv2, *Strep*-hIntL-1 was diluted to 50 μg/mL in binding buffer (20 mM Tris-HCl (7.4), 150 mM NaCl, 2 mM $CaCl_2$, 2 mM magnesium chloride ($MgCl_2$) 1% BSA, and 0.05% Tween-20) and applied directly to the array surface for 1 hour. Following incubation, the array was washed by dipping into binding buffer four times. The *Strep*-tag® II on bound hIntL-1 was detected using StrepMAB-Classic Chromeo647 nm (10 μg /mL, IBA GmbH Lifesciences) diluted in binding buffer applied directly to the array surface and allowed to incubate for 1 hour. The array was washed in binding buffer (4 dips), binding buffer minus BSA and Tween-20 (4 dips) and de-ionized water (4 dips). Finally, the array was dried by centrifugation and scanned. Interrogated arrays were scanned for Chromeo647 signal using a ProScanArray Express scanner (Perkin Elmer) and resultant images were processed to extract signal data using Imagene (v6.0, Biodiscovery). Signal data was calculated as the average of 4 values after removing the high and low values of the 6 replicates. Data were plotted using Excel (Microsoft) as average Relative Fluorescence

Units (RFU) versus print identification number. Figures were made using Prism6 (GraphPad).

Protein X-ray crystallography

The *Strep*-hIntL-1 protein that was purified using 20 mM BIS-TRIS (6.7) buffers, was concentrated to 1.5 mg/mL, 1 M $CaCl_2$ was added to a final concentration of 10 mM, and crystallization (hanging-drop vapor-diffusion) was achieved by mixing 1 μL of the protein solution and 1 μL of well solution (100 mM BIS-TRIS (6.0) and 25% PEG 3350). Crystals grew to full size in two weeks. Protein crystals of Apo-hIntL-1 were cryoprotected via transfer to well solution supplemented to a total concentration of 35% PEG 3350 for one minute and then vitrified in liquid nitrogen. The allyl-β-Gal*f*-hIntL-1 complex was formed by soaking apo-hIntL-1 crystals in cryoprotection solution supplemented with 50 mM allyl-β-D-galactofuranose for two weeks.

Single crystal X-ray diffraction experiments were performed at beamline 21-ID-D (Life Sciences Collaborative Access Team, LS-CAT), Advanced Photon Source, Argonne National Laboratory. The wavelength for data collection was 0.97924 Å for the Apo-hIntL-1 structure and 1.00394 for Gal*f*-Bound hIntL-1. Integration, scaling, and merging were performed with HKL2000[63]. The structure was solved using the PHENIX suite[64]. The *Xenopus laevis* intelectin structure recently solved in our lab was used as a search model to determine the structure of apo-hIntL-1 by molecular replacement using Phaser[65]. Because the apo-hIntL-1 and β-Gal*f*–bound hIntL-1 data are isomorphous, the structure of β-Gal*f*–bound hIntL-1 was solved by a difference Fourier method using apo-hIntL-1 as a starting model for rigid-body refinement with phenix.refine[66]. The chemical restraint for β-Gal*f* was generated by PRODRG[67]. Model adjustment and refinement were performed in Coot and phenix.refine, respectively (Supplemental Table 1)[68]. The model was validated using MolProbity[69]. Crystal structure figures were generated with PyMOL (http://www.pymol.org).

hIntL-1 binding to *Streptococcus pneumoniae*

Streptococcus pneumoniae (Klein) Chester serotype 8 (ATCC® 6308™), 20 (ATCC® 6320™), 43 (ATCC® 10343™) and 70 (ATCC® 10370™) were obtained from the ATCC. The structure of the capsular polysaccharide from each of these serotypes has been previously determined[46]. Cells were revived in trypic soy broth containing 5% defibrinated sheep blood. Cells were grown on plates of trypic soy agar containing 5% defibrinated sheep or in suspension in Luria Broth (LB). Cells were grown at 37 °C supplemented with 5% carbon dioxide gas. During liquid culture, cells were shaken at 100 RPM. To analyze hIntL-1 binding to the bacterial cell surface, cells were harvested by centrifugation, washed with PBS and fixed in 1% formaldehyde in PBS for 30 minutes on ice. Cells were stained with 15 μg/mL *Strep*-hIntL-1 with a 1:250 dilution of StrepMAB-Classic Oyster 645 conjugate (IBA GmbH, cat. no. 2–1555-050) in 20 mM HEPES (7.4), 150 mM NaCl, 10 mM $CaCl_2$, 0.1% BSA and 0.05% Tween-20 for 2 hours at 4 °C. To test the calcium ion dependency of binding, 20 mM HEPES (7.4), 150 mM NaCl, 10 mM EDTA, 0.1% BSA and 0.05% Tween-20 was used as the buffer. To assay for competitive inhibition by soluble glycerol, 20 mM HEPES (7.4), 150 mM NaCl, 10 mM $CaCl_2$, 100 mM glycerol, 0.1% BSA

and 0.05% Tween-20 was used as the buffer. Cells were washed with 20 mM HEPES (7.4), 150 mM NaCl, 10 mM $CaCl_2$, 0.1% BSA and 0.05% Tween-20, aggregates were removed with a flow cytometry cell-strainer cap (Falcon), and propidium iodide (Life Technologies) was added to a 1:500 dilution. Cells were analyzed on a BD FACSCalibur (Becton, Dickinson and Company) at the University of Wisconsin–Madison Carbone Canter Center (UWCCC) Flow Cytometry Laboratory. Propidium iodide was used to differentiate fixed *S. pneumoniae* cells from debris. Data was analyzed using FlowJo (FlowJo, LLC, Ashland, OR).

For analysis by microscopy, cell aliquots were taken directly from the flow cytometry samples prior to propidium iodide staining. Samples were subsequently stained with Hoechst 33342 (Life Technologies). Each sample was spotted onto a glass bottom microwell dish (MatTek corporation) and covered with a 1% (w/v) agarose pads prepared in a matched buffer. Images were collected at room temperature using a Nikon A1 laser scanning confocal microscope (Nikon Instruments Inc.). Images were acquired using a Nikon plan apo 100/1.4 oil objective using a 1.2 AU pinhole diameter and NIS-elements C software (Nikon Instruments Inc.). Laser setting were determined by imaging the brightest control sample, serotype 43 treated with 15 μg/mL *Strep*-hIntL-1 and a 1:250 dilution of StrepMAB-Classic Oyster 645 conjugate in calcium buffer, to prevent pixel oversaturation. The pinhole diameter, offset, PMT gain, and laser power were then held constant for each prepared sample. Each image was taken at the Z-plane that provided maximal signal for the given section. For Hoechst 33258, illumination was performed using a 405 nm laser and emission was collected between 425 and 475 nm. For StrepMAB-Classic Oyster 645 conjugate, illumination was performed using a 638 nm laser and emission was collected between 663 and 738 nm. Images were prepared using the open source Fiji distribution of ImageJ, brightness and contrast were adjusted in the control sample (serotype 43 treated with 15 μg/mL *Strep*-hIntL-1 with a 1:250 dilution of StrepMAB-Classic Oyster 645 conjugate in calcium buffer) and propagated to all selected sample images for comparison. Images were then converted to an RGB format to preserve normalization and then assembled into panels.

Expression of murine intelectin-1

A detailed description mIntL-1 expression is available in the Supplementary Note.

Supplementary Material

Refer to Web version on PubMed Central for supplementary material.

ACKNOWLEDGEMENTS

This research was supported by the US National Institutes of Health (NIH) (R01GM55984 and R01AI063596 (LLK)). D.A.W thanks the US National Science Foundation (NSF) and the NIH Chemistry–Biology Interface Training Program (T32 GM008505) for fellowships. K.W. was supported by a fellowship from the Development and Promotion of Science and Technology Talents Project of Thailand. The glycan array experiments were made possible by the Consortium for Functional Glycomics (NIGMS GM062116 and GM98791 (JCP)), which supported the Glycan Array Synthesis Core at The Scripps Research Institute, La Jolla, CA and the Protein-Glycan Interaction Resource (Emory University School of Medicine, Atlanta, GA). These resources assisted with analysis of samples on the array. Printing and processing the furanoside array was supported through the National Center for Functional Glycomics supported by NIGMS (P41GM103694 (RDC)). Surface plasmon resonance experiments were performed

at the UW–Madison Biophysics Instrumentation Facility, which is supported by UW-Madison, NSF grant BIR-9512577, and NIH grant S10 RR13790. Flow cytometry data were obtained at the UW-Madison Carbone Cancer Center (P30 CA014520) and microscopy images were acquired at the UW–Madison W.M. Keck Laboratory for Biological Imaging (1S10RR024715). The UW–Madison Chemistry NMR facility is supported by the NSF (CHE-9208463, CHE-9629688) and NIH (1s10 RR08389). Use of the Advanced Photon Source at the Argonne National Laboratory, was supported by the US Department of Energy (Contract DE-AC02-06CH11357) and the LS-CAT Sector 21 was supported by the Michigan Economic Development Corporation and the Michigan Technology Tri-Corridor (Grant 085P1000817). We thank J.M. Fishman for assistance preparing the synthetic methods, and M.R. Levengood, A.H. Courtney, and D.R. McCaslin for thoughtful discussions. We thank M.R. Richards (Univ. Alberta) for helpful discussions.

References

1. Stowell SR, et al. Innate immune lectins kill bacteria expressing blood group antigen. Nat. Med. 2010; 16:295–301. [PubMed: 20154696]
2. Vaishnava S, et al. The antibacterial lectin RegIIIgamma promotes the spatial segregation of microbiota and host in the intestine. Science. 2011; 334:255–258. [PubMed: 21998396]
3. Gallo RL, Hooper LV. Epithelial antimicrobial defence of the skin and intestine. Nat. Rev. Immunol. 2012; 12:503–516. [PubMed: 22728527]
4. Backhed F, Ley RE, Sonnenburg JL, Peterson DA, Gordon JI. Host-bacterial mutualism in the human intestine. Science. 2005; 307:1915–1920. [PubMed: 15790844]
5. Varki, A. Essentials of glycobiology. Cold Spring Harbor, N.Y.: Cold Spring Harbor Laboratory Press; 2009. p. 784
6. Lis H, Sharon N. Lectins: Carbohydrate-specific proteins that mediate cellular recognition. Chem. Rev. 1998; 98:637–674. [PubMed: 11848911]
7. Weis WI, Drickamer K. Structural basis of lectin-carbohydrate recognition. Annu. Rev. Biochem. 1996; 65:441–473. [PubMed: 8811186]
8. Turner MW. The role of mannose-binding lectin in health and disease. Mol. Immunol. 2003; 40:423–429. [PubMed: 14568388]
9. Fujita T. Evolution of the lectin-complement pathway and its role in innate immunity. Nat. Rev. Immunol. 2002; 2:346–353. [PubMed: 12033740]
10. Jack DL, Klein NJ, Turner MW. Mannose-binding lectin: targeting the microbial world for complement attack and opsonophagocytosis. Immunol. Rev. 2001; 180:86–99. [PubMed: 11414367]
11. Thomsen T, Schlosser A, Holmskov U, Sorensen GL. Ficolins and FIBCD1: soluble and membrane bound pattern recognition molecules with acetyl group selectivity. Mol. Immunol. 2011; 48:369–381. [PubMed: 21071088]
12. Holmskov U, Thiel S, Jensenius JC. Collectins and ficolins: Humoral lectins of the innate immune defense. Annu. Rev. Immunol. 2003; 21:547–578. [PubMed: 12524383]
13. Lehotzky RE, et al. Molecular basis for peptidoglycan recognition by a bactericidal lectin. Proc. Natl. Acad. Sci. U.S.A. 2010; 107:7722–7727. [PubMed: 20382864]
14. Lee JK, et al. Cloning and expression of a Xenopus laevis oocyte lectin and characterization of its mRNA levels during early development. Glycobiology. 1997; 7:367–372. [PubMed: 9147045]
15. Lee JK, Baum LG, Moremen K, Pierce M. The X-lectins: a new family with homology to the Xenopus laevis oocyte lectin XL-35. Glycoconjugate J. 2004; 21:443–450.
16. Weis WI, Taylor ME, Drickamer K. The C-type lectin superfamily in the immune system. Immunol. Rev. 1998; 163:19–34. [PubMed: 9700499]
17. Tsuji S, et al. Human intelectin is a novel soluble lectin that recognizes galactofuranose in carbohydrate chains of bacterial cell wall. J. Biol. Chem. 2001; 276:23456–23463. [PubMed: 11313366]
18. French AT, et al. The expression of intelectin in sheep goblet cells and upregulation by interleukin-4. Vet. Immunol. Immunopathol. 2007; 120:41–46. [PubMed: 17727963]
19. Voehringer D, et al. Nippostrongylus brasiliensis: identification of intelectin-1 and −2 as Stat6-dependent genes expressed in lung and intestine during infection. Exp. Parasitol. 2007; 116:458–466. [PubMed: 17420014]

20. Pemberton AD, Knight PA, Wright SH, Miller HR. Proteomic analysis of mouse jejunal epithelium and its response to infection with the intestinal nematode, Trichinella spiralis. Proteomics. 2004; 4:1101–1108. [PubMed: 15048991]
21. Datta R, et al. Identification of novel genes in intestinal tissue that are regulated after infection with an intestinal nematode parasite. Infect. Immun. 2005; 73:4025–4033. [PubMed: 15972490]
22. Kerr SC, et al. Intelectin-1 is a prominent protein constituent of pathologic mucus associated with eosinophilic airway inflammation in asthma. Am. J. Respir. Crit. Care Med. 2014; 189:1005–1007. [PubMed: 24735037]
23. Kuperman DA, et al. Dissecting asthma using focused transgenic modeling and functional genomics. J. Allergy Clin. Immunol. 2005; 116:305–311. [PubMed: 16083784]
24. Suzuki YA, Shin K, Lonnerdal B. Molecular cloning and functional expression of a human intestinal lactoferrin receptor. Biochemistry. 2001; 40:15771–15779. [PubMed: 11747454]
25. Tsuji S, et al. Secretion of intelectin-1 from malignant pleural mesothelioma into pleural effusion. Br. J. Cancer. 2010; 103:517–523. [PubMed: 20628387]
26. de Souza Batista CM, et al. Omentin plasma levels and gene expression are decreased in obesity. Diabetes. 2007; 56:1655–1661. [PubMed: 17329619]
27. Tsuji S, et al. Differential structure and activity between human and mouse intelectin-1: Human intelectin-1 is a disulfide-linked trimer, whereas mouse homologue is a monomer. Glycobiology. 2007; 17:1045–1051. [PubMed: 17621593]
28. Pedersen LL, Turco SJ. Galactofuranose metabolism: a potential target for antimicrobial chemotherapy. Cell. Mol. Life Sci. 2003; 60:259–266. [PubMed: 12678491]
29. Nassau PM, et al. Galactofuranose biosynthesis in Escherichia coli K-12: identification and cloning of UDP-galactopyranose mutase. J. Bacteriol. 1996; 178:1047–1052. [PubMed: 8576037]
30. Wesener DA, May JF, Huffman EM, Kiessling LL. UDP-galactopyranose mutase in nematodes. Biochemistry. 2013; 52:4391–4398. [PubMed: 23697711]
31. Bishop JR, Gagneux P. Evolution of carbohydrate antigens--microbial forces shaping host glycomes? Glycobiology. 2007; 17:23R–34R.
32. Herget S, et al. Statistical analysis of the Bacterial Carbohydrate Structure Data Base (BCSDB): characteristics and diversity of bacterial carbohydrates in comparison with mammalian glycans. BMC Struct. Biol. 2008; 8:35. [PubMed: 18694500]
33. Adibekian A, et al. Comparative bioinformatics analysis of the mammalian and bacterial glycomes. Chem. Sci. 2011; 2:337–344.
34. Mann DA, Kanai M, Maly DJ, Kiessling LL. Probing low affinity and multivalent interactions with surface plasmon resonance: Ligands for concanavalin A. J. Am. Chem. Soc. 1998; 120:10575–10582.
35. Kiessling LL, Grim JC. Glycopolymer probes of signal transduction. Chem. Soc. Rev. 2013; 42:4476–4491. [PubMed: 23595539]
36. Blixt O, et al. Printed covalent glycan array for ligand profiling of diverse glycan binding proteins. Proc. Natl. Acad. Sci. U.S.A. 2004; 101:17033–17038. [PubMed: 15563589]
37. Tefsen B, Ram AF, van Die I, Routier FH. Galactofuranose in eukaryotes: aspects of biosynthesis and functional impact. Glycobiology. 2012; 22:456–469. [PubMed: 21940757]
38. Stowell SR, et al. Microbial glycan microarrays define key features of host-microbial interactions. Nat. Chem. Biol. 2014; 10:470–476. [PubMed: 24814672]
39. Holm L, Rosenstrom P. Dali server: conservation mapping in 3D. Nucleic Acids Res. 2010; 38:W545–W549. [PubMed: 20457744]
40. Garlatti V, et al. Structural insights into the innate immune recognition specificities of L- and H-ficolins. EMBO J. 2007; 26:623–633. [PubMed: 17215869]
41. Taha HA, Richards MR, Lowary TL. Conformational analysis of furanoside-containing mono- and oligosaccharides. Chem. Rev. 2013; 113:1851–1876. [PubMed: 23072490]
42. Richards MR, Bai Y, Lowary TL. Comparison between DFT- and NMR-based conformational analysis of methyl galactofuranosides. Carbohyd. Res. 2013; 374:103–114.

43. Altona C, Sundaral M. Conformational-Analysis of Sugar Ring in Nucleosides and Nucleotides - New Description Using Concept of Pseudorotation. J. Am. Chem. Soc. 1972; 94:8205. [PubMed: 5079964]
44. Angata T, Varki A. Chemical diversity in the sialic acids and related alpha-keto acids: an evolutionary perspective. Chem. Rev. 2002; 102:439–469. [PubMed: 11841250]
45. Cartwright K. Pneumococcal disease in western Europe: burden of disease, antibiotic resistance and management. Eur. J. Pediatr. 2002; 161:188–195. [PubMed: 12014384]
46. Bentley SD, et al. Genetic analysis of the capsular biosynthetic locus from all 90 pneumococcal serotypes. PLoS Genet. 2006; 2:262–269.
47. Black S, et al. Efficacy, safety and immunogenicity of heptavalent pneumococcal conjugate vaccine in children. Pediatr. Infect. Dis. J. 2000; 19:187–195. [PubMed: 10749457]
48. Arnold RR, Cole MF, McGhee JR. A bactericidal effect for human lactoferrin. Science. 1977; 197:263–265. [PubMed: 327545]
49. Alexander DB, Iigo M, Yamauchi K, Suzui M, Tsuda H. Lactoferrin: an alternative view of its role in human biological fluids. Biochem. Cell. Biol. 2012; 90:279–306. [PubMed: 22553915]
50. Arnold RR, Russell JE, Champion WJ, Gauthier JJ. Bactericidal activity of human lactoferrin: influence of physical conditions and metabolic state of the target microorganism. Infect. Immun. 1981; 32:655–660. [PubMed: 7251141]
51. Asensio JL, Arda A, Canada FJ, Jimenez-Barbero J. Carbohydrate-aromatic interactions. Acc. Chem. Res. 2013; 46:946–954. [PubMed: 22704792]
52. Pemberton AD, Rose-Zerilli MJ, Holloway JW, Gray RD, Holgate ST. A single-nucleotide polymorphism in intelectin 1 is associated with increased asthma risk. J. Allergy Clin. Immunol. 2008; 122:1033–1034. [PubMed: 19000584]
53. Barrett JC, et al. Genome-wide association defines more than 30 distinct susceptibility loci for Crohn's disease. Nat. Genet. 2008; 40:955–962. [PubMed: 18587394]
54. Schnaitman CA, Klena JD. Genetics of lipopolysaccharide biosynthesis in enteric bacteria. Microbiol. Rev. 1993; 57:655–682. [PubMed: 7504166]
55. Willis LM, et al. Conserved glycolipid termini in capsular polysaccharides synthesized by ATP-binding cassette transporter-dependent pathways in Gram-negative pathogens. Proc. Natl. Acad. Sci. U.S.A. 2013; 110:7868–7873. [PubMed: 23610430]
56. Varghese JN, Mckimmbreschkin JL, Caldwell JB, Kortt AA, Colman PM. The Structure of the Complex between Influenza-Virus Neuraminidase and Sialic-Acid, the Viral Receptor. Proteins. 1992; 14:327–332. [PubMed: 1438172]
57. Kraschnefski MJ, et al. Effects on sialic acid recognition of amino acid mutations in the carbohydrate-binding cleft of the rotavirus spike protein. Glycobiology. 2009; 19:194–200. [PubMed: 18974199]
58. Blanchard H, Yu X, Coulson BS, von Itzstein M. Insight into host cell carbohydrate-recognition by human and porcine rotavirus from crystal structures of the virion spike associated carbohydrate-binding domain (VP8*). J. Mol. Biol. 2007; 367:1215–1226. [PubMed: 17306299]
59. Dormitzer PR, Sun ZYJ, Wagner G, Harrison SC. The rhesus rotavirus VP4 sialic acid binding domain has a galectin fold with a novel carbohydrate binding site. EMBO. J. 2002; 21:885–897. [PubMed: 11867517]
60. Sauter NK, et al. Binding of Influenza-Virus Hemagglutinin to Analogs of Its Cell-Surface Receptor, Sialic-Acid - Analysis by Proton Nuclear-Magnetic-Resonance Spectroscopy and X-Ray Crystallography. Biochemistry. 1992; 31:9609–9621. [PubMed: 1327122]

Methods references

36. Blixt O, et al. Printed covalent glycan array for ligand profiling of diverse glycan binding proteins. Proc. Natl. Acad. Sci. U.S.A. 2004; 101:17033–17038. [PubMed: 15563589]
38. Stowell SR, et al. Microbial glycan microarrays define key features of host-microbial interactions. Nat. Chem. Biol. 2014; 10:470–476. [PubMed: 24814672]
46. Bentley SD, et al. Genetic analysis of the capsular biosynthetic locus from all 90 pneumococcal serotypes. PLoS Genet. 2006; 2:262–269.

61. Song X, Lasanajak Y, Xia B, Smith DF, Cummings RD. Fluorescent glycosylamides produced by microscale derivatization of free glycans for natural glycan microarrays. ACS Chem. Biol. 2009; 4:741–750. [PubMed: 19618966]

62. Heimburg-Molinaro J, Song X, Smith DF, Cummings RD. Preparation and analysis of glycan microarrays. Curr. Protoc. Protein Sci. 2011; 12(12):10. [PubMed: 21488041]

63. Otwinowski, Z.; Minor, W. Processing of x-ray diffraction data collected in oscillation mode. In: Carter J, CW.; Sweet, RM., editors. in Methods Enzymol. Vol. 276. New York: Academic Press; 1997. p. 307-326.

64. Adams PD, et al. PHENIX: a comprehensive Python-based system for macromolecular structure solution. Acta Crystallogr., Sect. D: Biol. Crystallogr. 2010; 66:213–221. [PubMed: 20124702]

65. McCoy AJ, et al. Phaser crystallographic software. J. Appl. Crystallogr. 2007; 40:658–674. [PubMed: 19461840]

66. Afonine PV, Grosse-Kunstleve RW, Adams PD. The Phenix refinement framework. CCP4 Newsl. 2005; 42:48.

67. Schuttelkopf AW, van Aalten DM. PRODRG: a tool for high-throughput crystallography of protein-ligand complexes. Acta Crystallogr., Sect. D: Biol. Crystallogr. 2004; 60:1355–1363. [PubMed: 15272157]

68. Emsley P, Lohkamp B, Scott WG, Cowtan K. Features and development of Coot. Acta Crystallogr., Sect. D: Biol. Crystallogr. 2010; 66:486–501. [PubMed: 20383002]

69. Chen VB, et al. MolProbity: all-atom structure validation for macromolecular crystallography. Acta Crystallogr., Sect. D: Biol. Crystallogr. 2010; 66:12–21. [PubMed: 20057044]

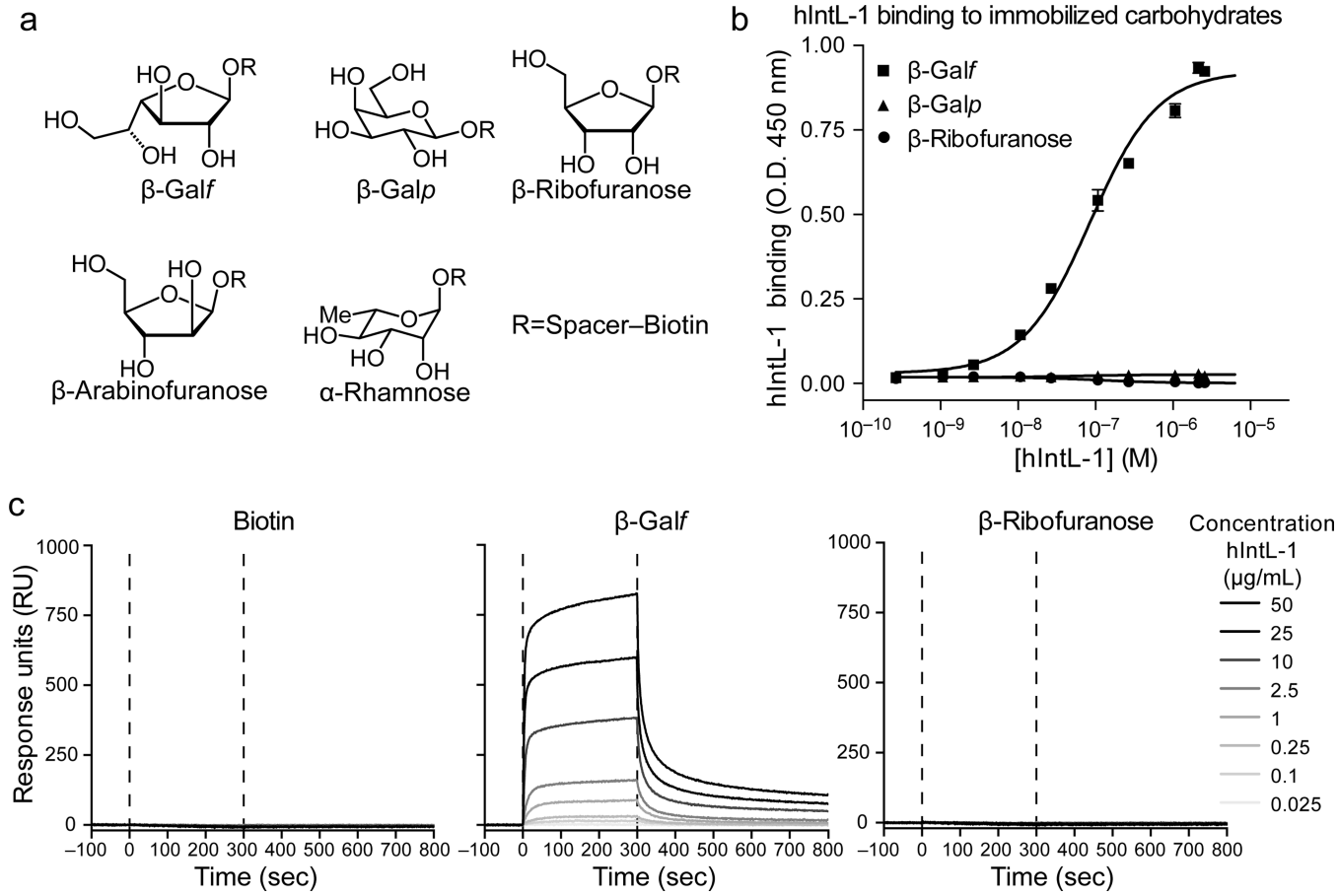

Figure 1.

hIntL-1 selectivity for monosaccharides. (**a**) Structures of saccharides used for characterization of hIntL-1 by ELISA and SPR. (**b**) The specificity of hIntL-1 for β-Gal*f*, β-ribofuranose (β-Rib*f*) and β-galactopyranose (β-Gal*p*) evaluated by ELISA (See Supplementary Fig. 1b for schematic). Data are presented as the mean ± s.d. (*n*=3 technical replicates, data are representative of >3 independent experiments). Data were fit to a single site binding equation (solid lines) and therefore represent the apparent (App) affinity of trimeric hIntL-1. Values for hIntL-1 bound to immobilized β-Gal*f* ($K_{d(App,\ Trimer)}$ ± s.d.) are 85 ± 14 nM or 8.0 ± 1.3 μg/mL. (**c**) Representative real-time SPR sensorgrams of hIntL-1 binding to immobilized carbohydrates. Biotin served as a control. The SPR complete data set is available in Supplementary Fig. 1e.

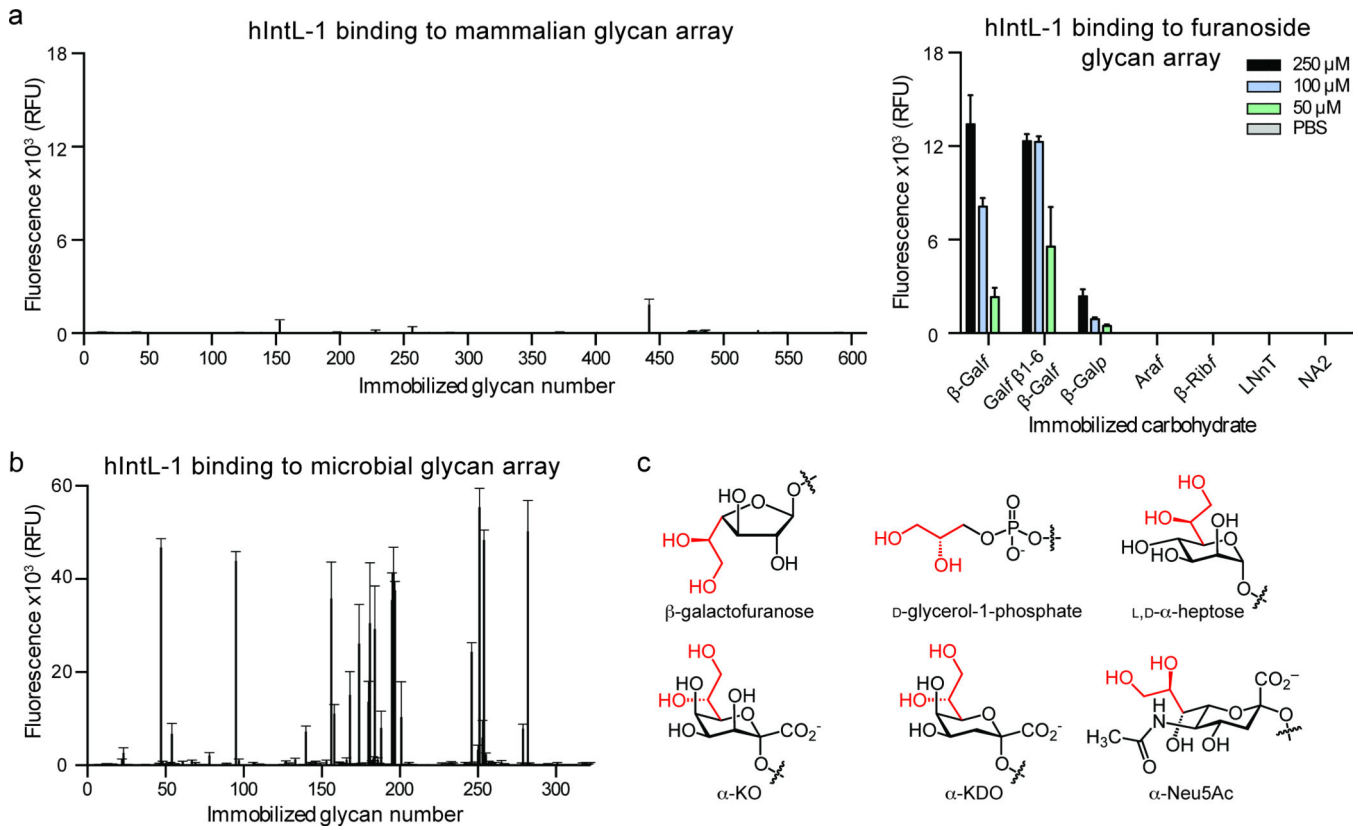

Figure 2.

Glycan selectivity of hIntL-1 assessed by glycan microarrays. (**a**) Recombinant hIntL-1 (50 μg/mL) binding to mammalian glycan microarray CFG v5.1 and a furanoside array. The concentrations given for the furanoside array represent those used in the carbohydrate immobilization reaction. Data are presented as the mean ± s.d. (*n*=4 technical replicates). The full data set can be found in Supplementary Tables 1 and 2. (**b**) Recombinant *Strep*-hIntL-1 (50 μg/mL) binding to microbial glycan array. For glycan array data organized by genus, see Supplementary Fig. 2a. Data are presented as the mean ± s.d. (*n*=4 technical replicates). The full data set can be found in Supplementary Table 3. (**c**) Structural representation of the putative key binding epitopes for hIntL-1 and the non-binding N-acetylneuraminic acid (α-Neu5Ac). A terminal vicinal diol (red) is a common feature of α-Neu5Ac and all of the ligands identified.

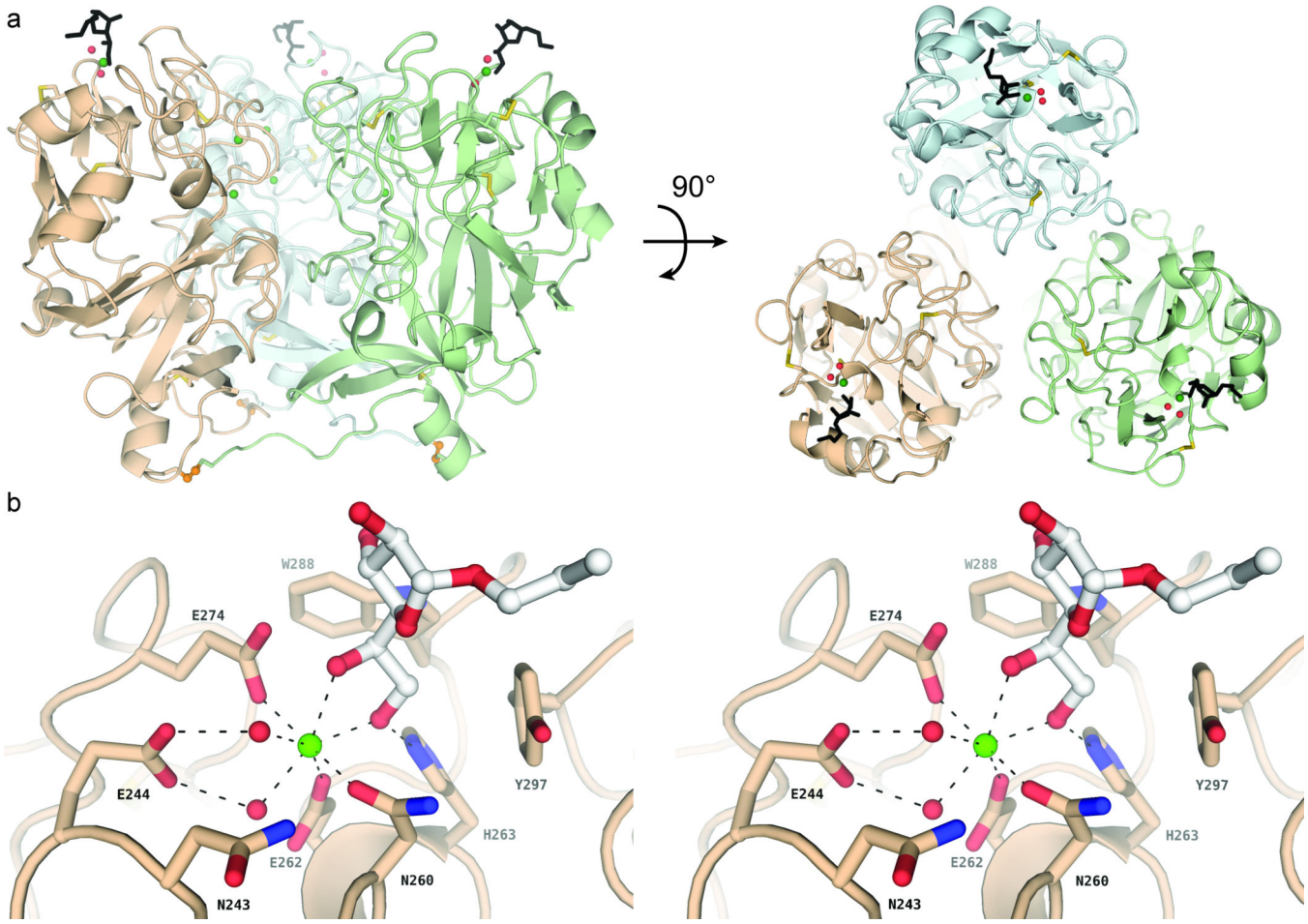

Figure 3.

Structure of hIntL-1 bound to allyl-β-D-Gal*f*. (**a**) Complex of hIntL-1 disulfide-linked trimer and allyl-β-D-Gal*f*. Each monomer unit is depicted in green, wheat, or grey, the β-allyl Gal*f* is shown in black, calcium ions in green, the inter-monomer disulfides in orange, and ordered water molecules in the binding site in red. The two orientations indicate the positioning of all three ligand-binding sites within the trimer. The trimeric structure is produced from Chain A in the asymmetric unit by a three-fold crystallographic operation. (**b**) Stereo image of the carbohydrate-binding site. Residues involved in calcium coordination and ligand binding are noted. Dashed lines are included to show the heptavalent coordination of the calcium ion and to highlight functional groups important for ligand and calcium ion binding. Difference density map (Fo-Fc, 3σ) of the allyl-β-D-Gal*f* ligand is provided in Supplementary Fig. 4b.

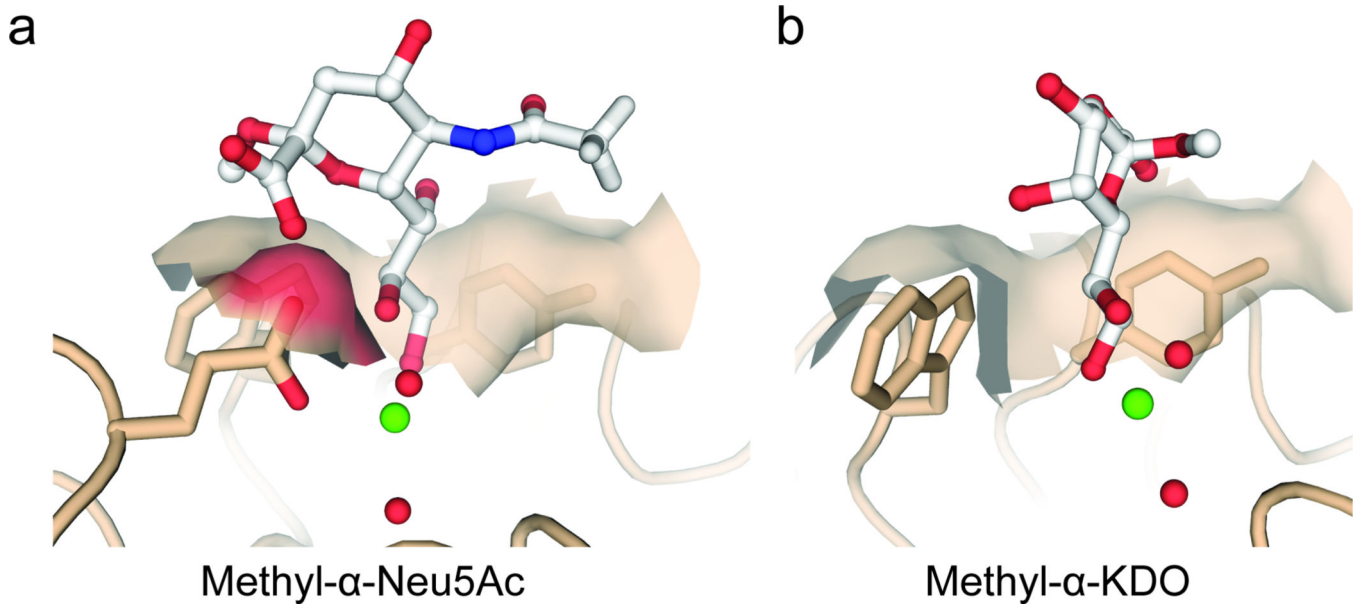

Figure 4.

Models for hIntL-1 interacting with relevant saccharide epitopes from humans (α-Neu5Ac) or microbes (α-KDO). (**a**) Docking of methyl-α-Neu5Ac into the hIntL-1 structure. The conformation shown is similar to that observed in other protein structures with a methyl-α-Neu5Ac ligand (PDB: 2BAT, 2P3I, 2P3J, 2P3K, 2I2S, 1KQR, 1HGE, 1HGH (refs. 56–60)). All models in this figure were generated from the allyl-β-D-Gal*f*–bound structure by docking the relevant diol of each compound into the Gal*f* diol electron density using Coot without further refinement. Calcium ions are shown in green and ordered water molecules are depicted in red. (**b**) Docking of methyl-α-KDO into the hIntL-1 structure. Comparison with methyl-α-Neu5Ac docked into the hIntL-1 structure reveal differences in the steric requirements for binding for each molecule.

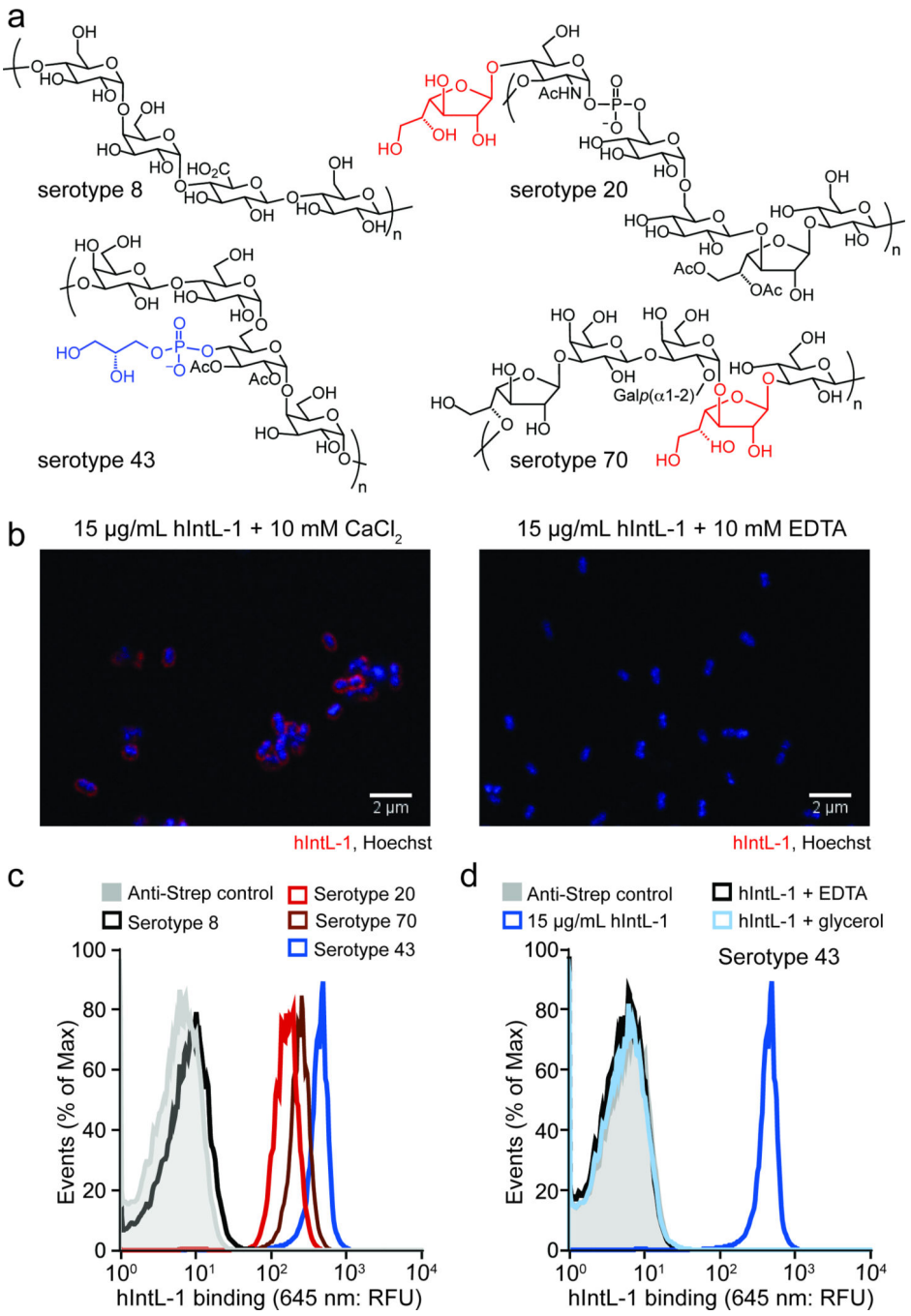

Figure 5.

Human IntL-1 binds to *S. pneumoniae* serotypes producing capsular polysaccharides with terminal vicinal diols. (**a**) Chemical structure of the capsular polysaccharides displayed on the *S. pneumoniae* serotypes (8, 20, 43, 70) tested. The Gal*f* residues assumed to mediate hIntL-1 cell binding are shown in red and the phosphoglycerol moiety is shown in blue. (**b**) Fluorescence microscopy of hIntL-1 binding to *S. pneumoniae* serotype 20. Bacteria were treated with Strep-tagged hIntL-1 (15 μg/mL) and an anti-Strep-tag antibody conjugate (red). Cellular DNA was visualized with Hoechst (blue). Left: hIntL-1 marks the surface of

serotype 20 bacteria; serotypes 43 and 70 gave similar results; no binding to serotype 8 was detected (Supplementary Fig. 6a) Right: EDTA addition abrogates hIntL-1 binding to the bacterial surface, supporting the role for Ca^{2+}. Images are representative of >5 fields of view per sample. Scale bar, 2 μm. (**c,d**) Flow cytometry analysis of Strep-hIntL-1 binding to *S. pneumoniae* serotypes with an anti-Strep-tag antibody conjugate. In the anti-Strep control sample, recombinant hIntL-1 was omitted. Cells were labeled with propidium iodide. (**c**) Flow cytometry analysis of serotypes 8, 20, 43, and 70; data were collected consecutively with identical instrument settings. (**d**) The dependence of the hIntL-1–carbohydrate interaction on Ca^{2+} was tested by adding 10 mM EDTA and ligand selectivity was tested by adding 100 mM glycerol. Data are representative of two independent experiments. For a similar analysis of serotypes 20 and 70 (no binding to serotype 8 was detected), see Supplementary Fig. 6b.

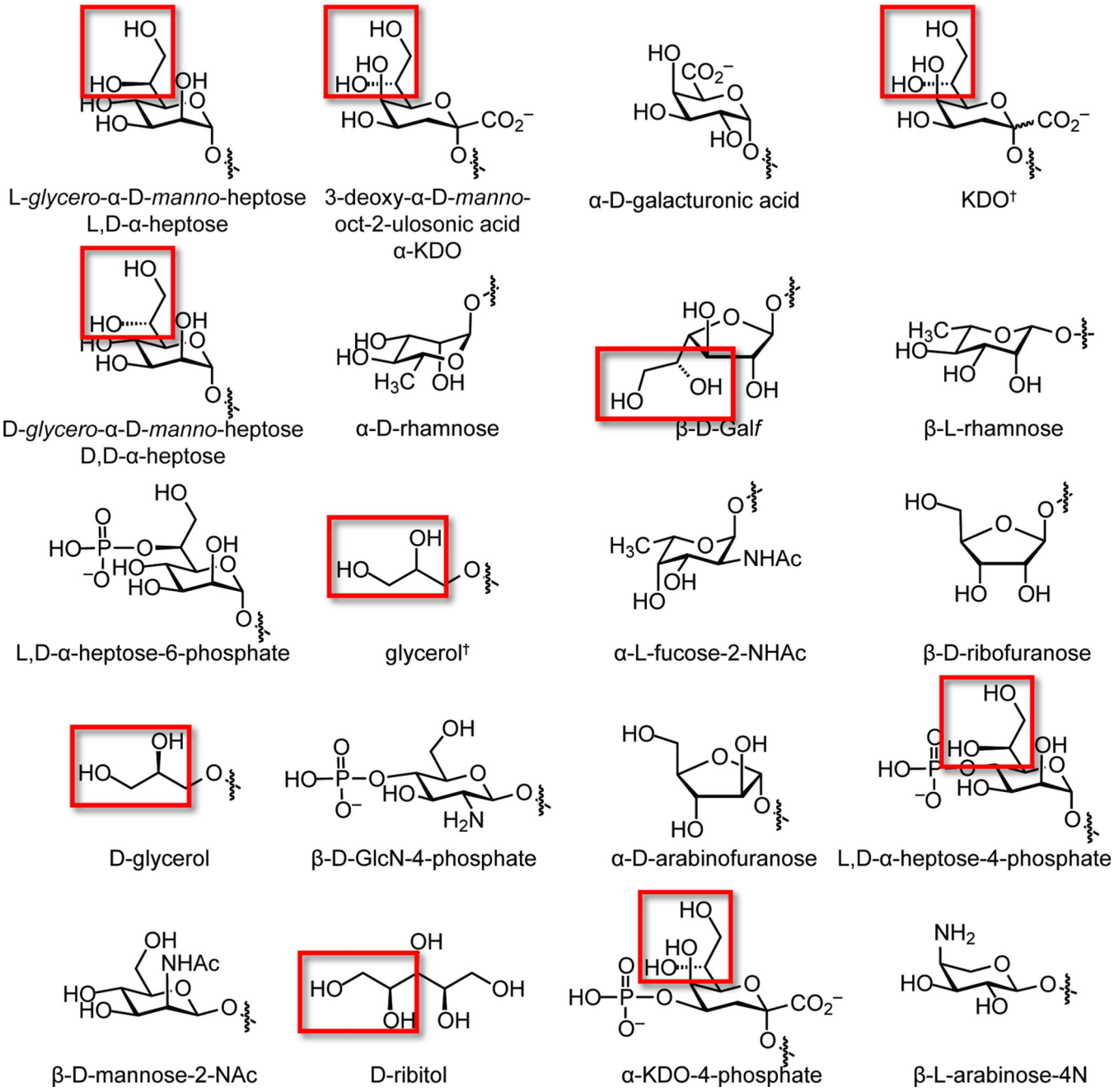

Figure 6.

Structures of the 20 most prevalent monosaccharides that are unique to bacterial glycans. The most common, l,d-α-heptose, is shown in the top left corner and number twenty, β-L-arabinose-4-N, is shown in the bottom right. This figure is derived from data in reference 32. Terminal acyclic 1,2-diol epitopes that could serve as ligands of hIntL-1 are highlighted with a red box.

Table 1

The list of the top 15 microbial glycan ligands, sorted by average fluorescence intensity (RFU).

Rank	Microbial sample	Proposed ligand
1	*S. pneumoniae* type 43	Glycerol–phosphate
2	*P. mirabilis* O54ab	Glycerol–phosphate
3	*S. pneumoniae* type 56	Glycerol–phosphate
4	*P. mirabilis* O54a, 54b	Glycerol–phosphate
5	*P. vulgaris* O54a, 54c	Glycerol–phosphate
6	*K. pneumoniae* O2a OPS	β-Gal*f*
7	*K. pneumoniae* O2ac OPS	β-Gal*f*
8	*Y. pestis* KM260(11)-Δ0187[a]	
9	*K. pneumoniae* O1 OPS	β-Gal*f*
10	*Y. pestis* 11M-37	Heptose, KO, KDO
11	*Y. pestis* KM260(11)-6C[a]	
12	*Y. pestis* KM260(11)-Δwaal	Heptose, KO, KDO
13	*S. pneumoniae* type 20	Heptose, KO, KDO
14	*Y. pestis* KM260(11)-ΔpmrF	Heptose, KO, KDO
15	*Y. pestis* 11M-25	Heptose, KO, KDO

[a]These glycans are currently structurally uncharacterized.

Table 2

Data collection and refinement statistics (molecular replacement)

	Apo-hIntL-1	Gal*f*-bound hIntL-1
Data collection		
Space group	P 2_1 3	P 2_1 3
Cell dimensions		
a,*b*,*c* (Å)	118.4, 118.4, 118.4	117.9, 117.9, 117.9
α,β, γ (°)	90, 90, 90	90, 90, 90
Resolution (Å)	22.00–1.80 (1.86–1.80)[a]	28.59-1.60 (1.66-1.60)
R_{sym}	0.119 (0.495)	0.078 (0.773)
I / σI	19.6 (3.7)	29.4 (3.0)
Completeness (%)	100 (100)	100 (100)
Redundancy	11.2 (10.1)	11.1 (10.9)
Refinement		
Resolution (Å)	22.00–1.80 (1.86–1.80)	28.59–1.60 (1.68–1.60)
No. reflections	48784	68256
R_{work} / R_{free}	0.133/ 0.164	0.155/0.180
No. atoms		
Protein	4551	4606
Ca^{2+}	6	6
Allyl-β-D-Gal*f*	-	30
Water	658	616
B-factors (Å^2)		
Protein	14.0	20.2
Ca^{2+}	10.1	14.5
Allyl-β-D-Gal*f*	-	33.8
Water	26.0	32.6
rms deviation		
Bond lengths (Å)	0.010	0.010
Bond angles (°)	1.107	1.119

Each data set was collected from one crystal.

[a] Values in parentheses are for highest-resolution shell.